

## Supplementary Information

### **Boosting photocatalytic removal of organic pollutants through enhanced piezoelectricity in freestanding nanofibril pyridyl-functionalized conjugated microporous polymer/poly(vinylidene fluoride-trifluoroethylene) hybrids**

Nan Meng<sup>a</sup>, Yu Zhang<sup>a</sup>, Yongsheng Liu<sup>a</sup>, Yu Shi<sup>a</sup>, Ruyu Jiang<sup>a</sup>, Jiyue Wu<sup>b</sup>, Yaozu Liao<sup>a\*</sup>

<sup>a</sup> State Key Laboratory for Modification of Chemical Fibers and Polymer Materials and College of Materials Science and Engineering, Donghua University, Shanghai, 21620, China.

<sup>b</sup> Department of Materials Science and State Key Laboratory of Molecular Engineering of Polymers, Fudan University, Shanghai, 200433, China

Corresponding author: yzliao@dhu.edu.cn

## **1. Experimental section**

### **1.1. Morphology and Structure Characterizations**

Scanning electron microscopy (SEM) was carried out on a HITACHI S-4800 microscope (Hitachi High-Technologies Corporation, Tokyo, Japan). Gold was sputtered before observation. The diameters of fibers were analyzed using ImageJ (National Institute of Health, USA). Transmission electron microscopy (TEM) and energy dispersive spectroscopy (EDS) were conducted on a JEM-2100 TEM microscope (Jeol Ltd., Tokyo, Japan). For TEM sample preparation, small pieces of fiber films were freeze-fractured in liquid nitrogen, and then transferred on ultrathin carbon films coated copper grids. X-ray photoelectron spectra (XPS) were obtained on a spectrometer of ESCALAB 250Xi (Thermo Fisher Scientific, Massachusetts, USA). Fourier transform infrared spectroscopy (FTIR) were achieved using attenuated total reflection (ATR) method on a Nicolet IS5 spectrometer (Thermo Fisher Scientific, Massachusetts, USA). X-ray diffraction (XRD) patterns in a  $2\theta$  range of  $5-90^\circ$  were

obtained on a Bruker D8 Advance diffractometer (Bruker Co., Massachusetts, USA). The value of zeta potential (ZS90, Malvern Panalytical Ltd, UK) was measured to analyze the underlying mechanism of surface functionalization of PCMPs.

### **1.2. Catalytic Performance Evaluation**

The piezo-photocatalytic behavior of m-PCMP powders and m-PCMP/PVDF-TrFE fiber films was evaluated *via* the decomposition of the organic dye of Rhodamine B (RhB) under UV irradiation (15 W). The periodic mechanical strain was driven using a portable ultrasound physiotherapy instrument under an irradiation of 1.5 W/cm<sup>2</sup> with a frequency of 1 MHz (Chattanooga Intelect, TN, USA). In a typical test, 40 mg fiber films or m-PCMP powders were dispersed in 40 mL RhB aqueous solution (initial concentration: 10 mg/L) and then the suspension was stirred in the dark at room temperature for 2 h to reach the equilibrium of adsorption-desorption between dyes and testing samples. 4 ml suspension was dispensed every 20 min of ultrasonication, and then centrifugal separated to get the supernatant liquid for measurement. The variation of the absorbance at 554 nm (characteristic peak of RhB) were monitored using UV-Vis absorption spectra (UV-3600, Shimadzu Co., Kyoto, Japan). The generation of OH and O<sub>2</sub><sup>-</sup> was confirmed using electron spin-resonance spectroscopy (ESR, EMX-8/2.7, Bruker Co., Massachusetts, USA). The piezoelectric characterization was determined using piezoresponse force microscopy (PFM) which were acquired on Bruker Dimension ICON system (Bruker Co., Massachusetts, USA), using a conductive tip with an AC electric field of 10 V.

### **1.3. Active Species Trapping Experiments**

The trapping experiments using different scavengers were carried out to confirm the responsible active species for the degradation of dyes during the piezocatalytic measurement. Silver nitrate (AgNO<sub>3</sub>, 10 mM), 1,4-benzoquinone (BQ, 5 mM), edetate disodium dehydrate (EDTA-2Na, 10 mM), and tert-butanol (TBA, 10 mM) are scavenger of electron (e<sup>-</sup>), superoxide radical ( $\cdot\text{O}_2^-$ ), hole (h<sup>+</sup>), and hydroxyl radical ( $\cdot\text{OH}$ ), respectively. Similar to the piezo-photocatalytic evaluation experiment, RhB (10 mg/L) was selected as the probe dye. 40 mg films were firstly added in 40 ml RhB aqueous solution (initial concentration: 10 mg/L). After reaching the equilibrium of

adsorption-desorption, different scavengers were added in the solution followed by the ultrasonication and UV irradiation. The degradation performance of RhB in the presence of scavengers was monitored using UV-Vis spectra every 20 min of ultrasonication, and more details have been described in section 1.2.

#### 1.4. $\cdot\text{OH}$ and $\cdot\text{O}_2^-$ Detection Using Electron Spin Resonance (ESR) Spectroscopy

ESR measurement was used to confirm the formation of  $\cdot\text{OH}$  and  $\cdot\text{O}_2^-$  during the piezo-photocatalysis of samples. 5, 5-dimethyl-1-pyrroline N-oxide (DMPO) was applied as the trapping agent. Testing samples (200 ppm) and DMPO (10  $\mu\text{L}$ ) were added in a 500  $\mu\text{L}$  ultrapure water or ethanol for detecting  $\cdot\text{OH}$  or  $\cdot\text{O}_2^-$ , respectively, followed by ultrasonication (1.5  $\text{W}/\text{cm}^2$ ) and UV irradiation (15 W) for 10 min. For comparison, pure DMPO with or without ultrasonication, and DMPO with samples but without sonication were used as control groups to highlight the piezo-photocatalytic effect.

#### 1.5. Band Gap Analysis of PCMP Before and After Surface Modification

The energy bandgap ( $E_g$ ) of PCMP and m-PCMP was estimated from the solid UV-Vis diffuse reflection spectrums using the Tauc plot *via* Kubelka-Munk equations<sup>1</sup>:

$$F(R)h\nu = A(h\nu - E_g)^n \quad (1)$$

$$F(R) = \frac{(1 - R)^2}{2R} \quad (2)$$

where  $F(R)$ ,  $R$ ,  $h$ ,  $\nu$  and  $A$  represent the Kubelka-Munk function, reflectance, the Planck's constant, frequency and a constant, respectively.  $n$  is 0.5 for direct bandgap semiconductor of PCMP.

The conduction band ( $E_{\text{CB}}$ ) of PCMP and m-PCMP was determined using Mott-Schottky plots which were measured on an Interface 1000E (Gamry Instruments, USA) electrochemical workstation using a standard three-electrode system (a working electrode, a counter electrode of platinum plate, and a reference electrode of Ag/AgCl).

The work electrodes were prepared as follows. PCMP or m-PCMP (50 mg) was

suspended in methanol solution (200  $\mu\text{L}$ ) followed by ultrasonication for 1 h. The as-prepared slurry (50  $\mu\text{L}$ ) was mixed with Nafion (50  $\mu\text{L}$ ), which was then dip-coated onto a glassy carbon electrode, and dried for 12 h. Mott-Schottky plots were measured using the method of impedance potential at 1000 Hz in 0.2 mol/L  $\text{Na}_2\text{SO}_4$  solution.

## 1.6. Detailed Parameters of COMSOL Finite Element Method (FEM)

### Simulation

The COMSOL Multiphysics® software (COMSOL Inc., USA) was used to simulate the piezo-potential of PVDF-TrFE under the hydroacoustic pressure. The simulation was built using the module of piezoelectricity interface and PVDF-TrFE fibers with a diameter of 200 nm and length of about 10  $\mu\text{m}$ , and an environment of water (dielectric permittivity  $\epsilon_r=80$ ). The density of PVDF-TrFE is defined as 1.78  $\text{g cm}^{-3}$ . The elastic matrix ( $cE$ ), coupling matrix ( $eES$ ), and  $\epsilon_r$  of PVDF-TrFE fibers are listed as below:

$$cE = \begin{pmatrix} 0.253 & 0 & 0 & 0 & 0 & 0 \\ -0.98 & 0.238 & 0 & 0 & 0 & 0 \\ -0.394 & -0.513 & 0.1 & 0 & 0 & 0 \\ 0 & 0 & 0 & 5.495 & 0 & 0 \\ 0 & 0 & 0 & 0 & 5.917 & 0 \\ 0 & 0 & 0 & 0 & 0 & 6.993 \end{pmatrix} \times 10^{11} \quad \text{Pa}$$

$$eES = \begin{pmatrix} 0 & 0 & 0 & 0 & -0.081 & 0 \\ 0 & 0 & 0 & -0.069 & 0 & 0 \\ 0.069 & 0.069 & -0.099 & 0 & 0 & 0 \end{pmatrix} \text{Cm}^{-2}$$

$$\epsilon_r = \begin{pmatrix} 10 & 0 & 0 \\ 0 & 10 & 0 \\ 0 & 0 & 10 \end{pmatrix}$$

The hydroacoustic pressure is set as 100 MPa. In the model of a single fiber, the pressure load was applied along the fiber axis. The pressure load was applied perpendicular to the surface of fiber film in the model of multiple fibers.

## 2. Supplementary Figures and Tables

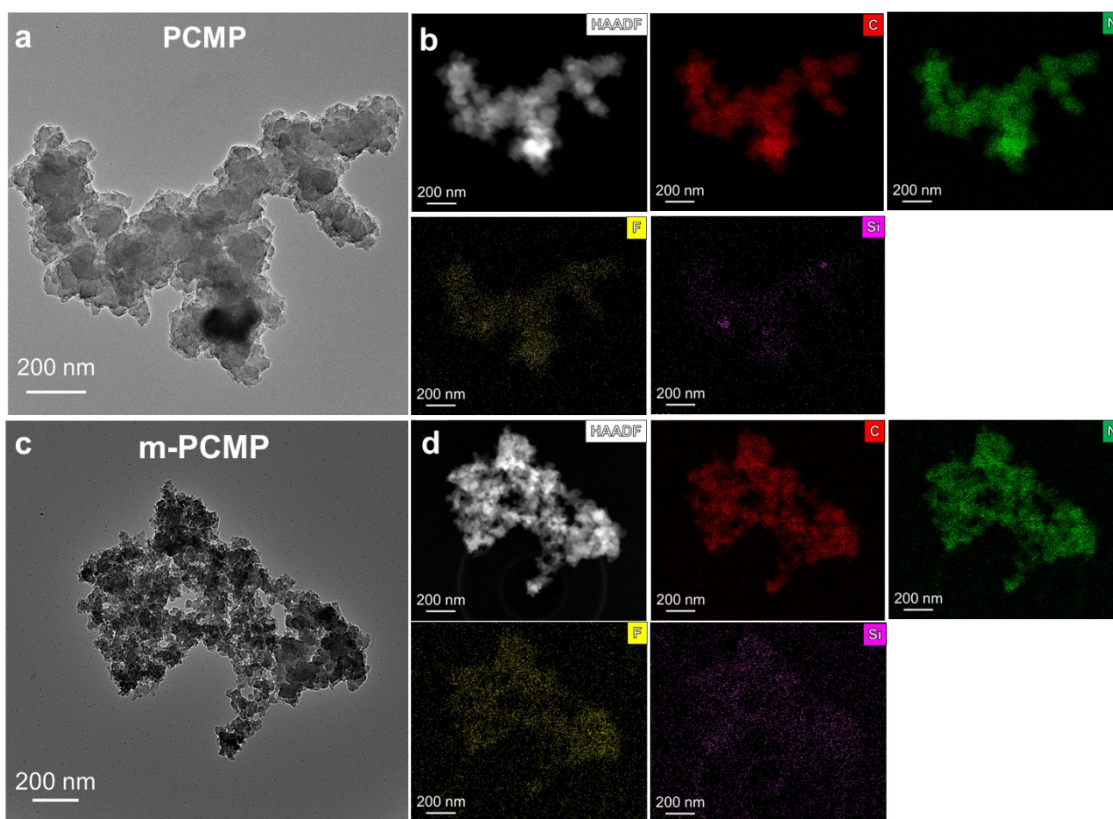
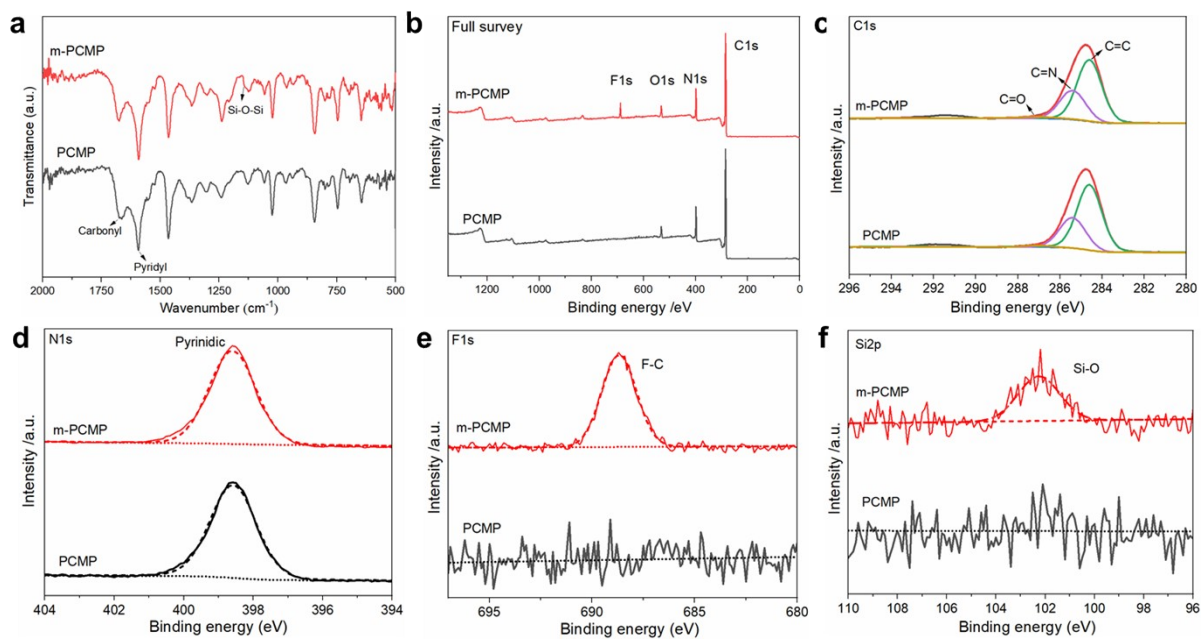


**Figure S1.** (a, c) TEM images and (b, d) HAADF images and its corresponding element



mapping images for original PCMP and m-PCMP, respectively.

**Figure S2** (a) FTIR spectra and (b-f) XPS spectra of PCMP and m-PCMP.

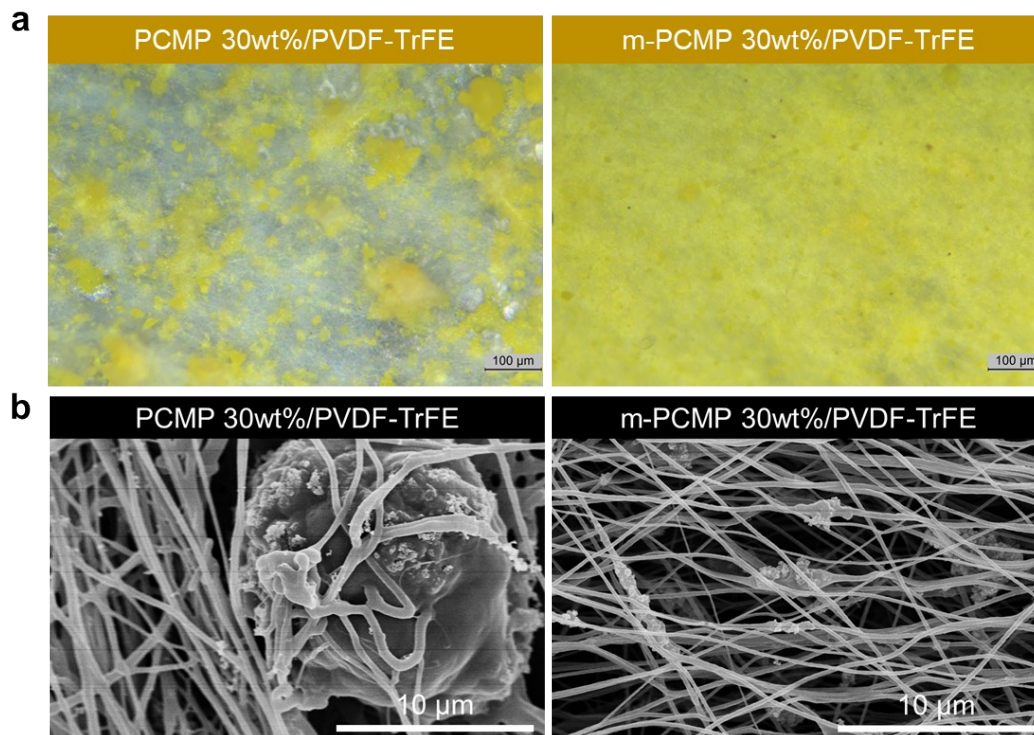


**Figure S3** The optical microscope images (a) and SEM images (b) of PCMP 30 wt%/PVDF-TrFE and m-PCMP 30 wt%/PVDF-TrFE, respectively.

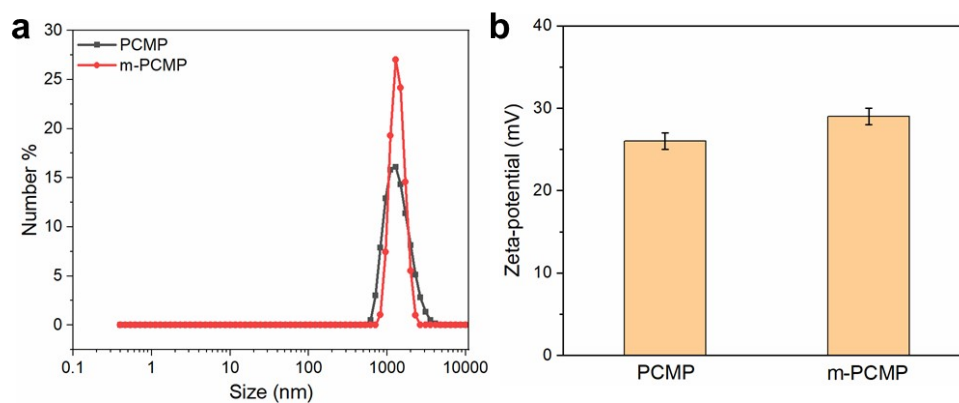


**Figure S4** The size distribution (a) and zeta-potential (b) of PCMP and m-PCMP measured at pH=7.

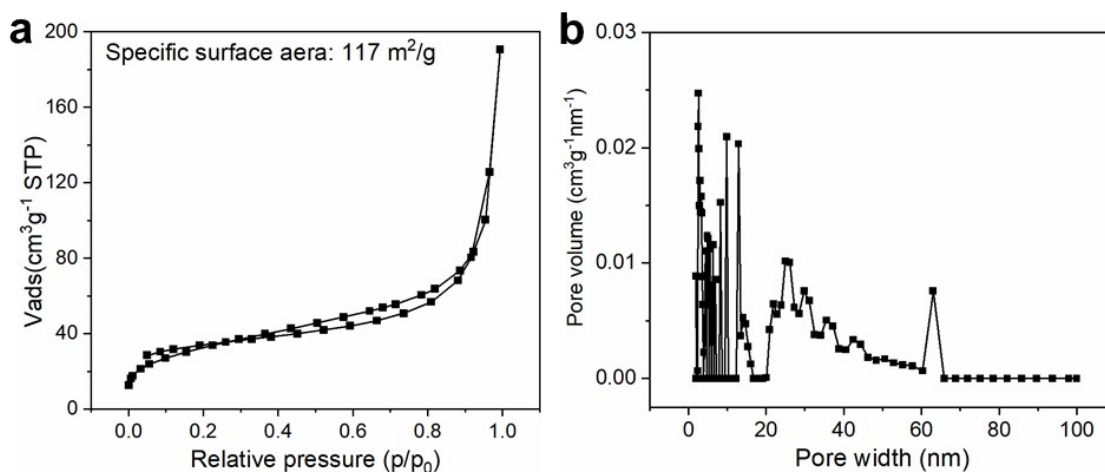


**Figure S5** (a) The N<sub>2</sub> adsorption/desorption isotherms at 77 K with specific surface area evaluated using the Brunauer-Emmett-Teller (BET) theory. (b) The pore size distribution derived based on the non-local density functional theory of m-PCMP.

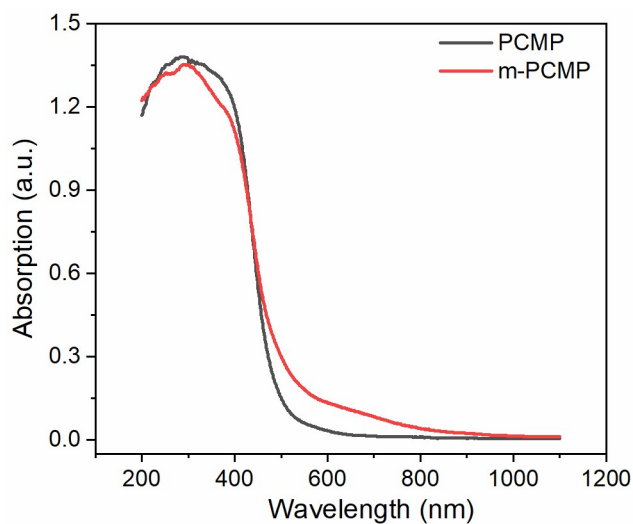


**Figure S6** The UV-Vis diffuse reflection spectra of PCMP and m-PCMP.

**Table S1.** The composition of different elements derived from EDS in PCMP and m-PCMP

Elements	PCMP		m-PCMP	
	Atomic %	Weight %	Atomic %	Weight %
C	85.9±5	83.0±3	85.6±5	80.1±5
N	12.8±3	14.4±3	9.8±2	10.6±2
F	0.5±0.1	0.8±0.2	0.9±0.2	1.3±0.3
Si	0.8±0.2	1.8±0.4	3.7±0.7	8.0±1.6
Total	100	100	100	100

**Table S2.** The local composition derived from EDS of single fibers in pure PVDF-TrFE, m-PCMP 50 wt%/PVDF-TrFE surrounded by m-PCMP fillers and beaded fibers.

Elements	PVDF-TrFE		m-PCMP 50 wt% -surrounded		m-PCMP 50 wt% -beaded fibers	
	Atomic (%)	Weight (%)	Atomic (%)	Weight (%)	Atomic (%)	Weight (%)
C	69.5±8	59.3±4	79.0±5	72.9±3	76.6±7	68.3±4
F	29.7±6	38.7±8	6.8±1	9.9±2	18.2±4	25.6±5
O	1.7±0.4	2±0.4	13.5±2	16.5±3	4.9±1	5.8±1
N	0	0	0.7±0.2	0.7±0.2	0.3±0.1	0.3±0.1
Total	100	100	100	100	100	100

Table S3 Comparison of the dye degradation performance of polymer-based piezocatalysts and piezo-photocatalysts.

Materials	ROS	Dye concentration and degradation efficiency	Catalytic conditions	Ref
Sn <sub>3</sub> O <sub>4</sub> /PVDF	•OH	RhB [2 mg L <sup>-1</sup> ], ~ 62.6%	Mercury lamp [150 W]; water flow [480 mL min <sup>-1</sup> ]; 225 min	2
BNT/PVDF foams	•OH, •O <sub>2</sub> <sup>-</sup>	RhB [5 mg L <sup>-1</sup> ], ~ 96%	Xe lamp [300 W]; Ultrasound [45 kHz, 200 W]; 30 min	3
ZnO/PVDF-HFP sponge	•OH, •O <sub>2</sub> <sup>-</sup>	MO [5 mg L <sup>-1</sup> ], ~ 95%	Mercury-xenon lamp [180 W]; Stirring [1000 rpm]; 75 min	4
TiO <sub>2</sub> @rGO-F/PVDF-HFP porous films		MO [1.8 mg L <sup>-1</sup> ], ~ 99%	Mercury lamp [300 W]; shaking water bath [80 rotation min <sup>-1</sup> ]; 60 min	5
KNN6L-PDMS porous foam	•OH, •O <sub>2</sub> <sup>-</sup>	RhB [5 mg L <sup>-1</sup> ], ~ 91%	Ultrasound [40 kHz, 180 W]; 180min	6
BaTiO <sub>3</sub> /PDMS porous foam	•OH, •O <sub>2</sub> <sup>-</sup>	RhB [5 mg L <sup>-1</sup> ], ~ 94%	Ultrasound [40 kHz, 400 W]; 120min	7

Ag@LiNbO <sub>3</sub> /PVDF	•OH	MB [5 mg L <sup>-1</sup> ], ~ 89%	Ultrasound [40 kHz, 70 W]; 120min	8
ZnSnO <sub>3</sub> /Co <sub>3</sub> O <sub>4</sub> /PVDF	•OH, •O <sub>2</sub> <sup>-</sup>	MB [5 mg L <sup>-1</sup> ], ~ 89%	Ultrasound [33 kHz, 120 W]; 20min	9
<b>m-PCMP 50 wt%/PVDF- TrFE</b>	<b>•OH</b>	<b>RhB [10 mg L<sup>-1</sup>], ~ 97%</b>	<b>UV irradiation [15 W]; Ultrasound [1 MHz, 7.0 W]; 30 min</b>	<b>Our work</b>

## Reference

1. A. A. Kokhanovsky, *Journal of Physics D: Applied Physics*, 2007, **40**, 2210-2216.
2. S. Han, D. Chen, J. Wang, Z. Liu, F. Liu, Y. Chen, Y. Ji, J. Pang, H. Liu and J. Wang, *Nano Energy*, 2020, **72**, 104688.
3. X. Zhou, Q. Sun, Z. Xiao, H. Luo and D. Zhang, *Journal of Environmental Chemical Engineering*, 2022, **10**, 108399.
4. R. Wang, X. Xie, C. Xu, Y. Lin, D. You, J. Chen, Z. Li, Z. Shi, Q. Cui and M. Wang, *Chemical Engineering Journal*, 2022, **439**, 135787.
5. W. Tong, Y. Zhang, H. Huang, K. Xiao, S. Yu, Y. Zhou, L. Liu, H. Li, L. Liu, T. Huang, M. Li, Q. Zhang, R. Du and Q. An, *Nano Energy*, 2018, **53**, 513-523.
6. X. Cheng, Z. Liu, Q. Jing, P. Mao, K. Guo, J. Lu, B. Xie and H. Fan, *Journal of Colloid and Interface Science*, 2023, **629**, 11-21.
7. W. Qian, K. Zhao, D. Zhang, C. R. Bowen, Y. Wang and Y. Yang, *ACS Applied Materials & Interfaces*, 2019, **11**, 27862-27869.
8. G. Singh, M. Sharma and R. Vaish, *ACS Applied Materials & Interfaces*, 2021, **13**, 22914-22925.
9. T. D. Raju, S. Veeralingam and S. Badhulika, *ACS Applied Nano Materials*, 2020, **3**, 4777-4787.